The Astrophysical Journal Supplement Series, 260:46 (15pp), 2022 June https://doi.org/10.3847/1538-4365/ac6676
© 2022. The Author(s). Published by the American Astronomical Society.
OPEN ACCESS

The OGLE Collection of Variable Stars: Nearly 66,000 Mira Stars in the Milky Way

Patryk Iwanek[1], Igor Soszyński[1], Szymon Kozłowski[1], Radosław Poleski[1], Paweł Pietrukowicz[1], Jan Skowron[1], Marcin Wrona[1], Przemysław Mróz[1], Andrzej Udalski[1], Michał K. Szymański[1], Dorota M. Skowron[1], Krzysztof Ulaczyk[1,2], Mariusz Gromadzki[1], Krzysztof Rybicki[1], and Milena Ratajczak[1]
[1] Astronomical Observatory, University of Warsaw, Al. Ujazdowskie 4, 00-478 Warsaw, Poland; piwanek@astrouw.edu.pl
[2] Department of Physics, University of Warwick, Coventry, CV4 7AL, UK
Received 2022 March 30; revised 2022 April 6; accepted 2022 April 8; published 2022 June 23

Abstract

We present a collection of 65,981 Mira-type variable stars found in the Optical Gravitational Lensing Experiment (OGLE) project database. Two-thirds of our sample (40,356 objects) are located in the Galactic bulge fields, whereas 25,625 stars are in the Galactic disk. The vast majority of the collection (47,532 objects) comprises new discoveries. We provide basic observational parameters of the Mira variables: equatorial coordinates, pulsation periods, *I*-band and *V*-band mean magnitudes, *I*-band brightness amplitudes, and identifications in other catalogs of variable stars. We also provide the *I*-band and *V*-band time-series photometry collected since 1997 during the OGLE-II, OGLE-III, and OGLE-IV phases. The classical selection process, i.e., being mostly based on the visual inspection of light curves by experienced astronomers, has led to the high purity of the catalog. As a result, this collection can be used as a training set for machine-learning classification algorithms. Using overlapping areas of adjacent OGLE fields, we estimate the completeness of the catalog to be about 96%. We compare and discuss the statistical features of Miras located in different regions of the Milky Way. We show examples of stars that change their type over time, from a semiregular variable to Mira and vice versa. This data set is perfectly suited to studying the three-dimensional structure of the Milky Way, and it may help to explain the puzzle of the X-shaped bulge.

Unified Astronomy Thesaurus concepts: Asymptotic giant branch stars (2100); Carbon stars (199); Mira variable stars (1066); Long period variable stars (935); Time series analysis (1916); Astrographic catalogs (77); Catalogs (205); Sky surveys (1464); Galactic bulge (2041); Galactic center (565); Milky Way Galaxy (1054); Milky Way disk (1050)

Supporting material: machine-readable tables

1. Introduction

The Mira star (*o* Ceti), named by Johannes Hevelius in 1662, in Latin means *wonderful, astonishing, miracle*. This name is not accidental, as in the sixteenth century, just after the discoveries of Mira's variability by David Fabricius and its periodicity by Johannes Holwarda, the regular appearance and disappearance of the celestial object had never been seen before. The Mira star has become a prototype of a numerous group of pulsating long-period variables (LPVs; Hogg 1933).

LPVs are mostly red-giant branch or asymptotic giant branch stars, but late-type pulsating supergiants (semiregular variables of c type) are also part of this group. During these evolutionary stages, stars are pulsationally unstable, which leads to their brightness changes with periods ranging from days to years. One of the subgroups of LPVs is Mira-type variables, which are perhaps the best-known LPVs, due to the history of their study spanning more than four centuries.

The first discovered Mira-type star, after *o* Ceti itself, was χ Cygni, discovered by Gottfried Kirch in 1686. Between 1686 and 1796, four Miras were known, and the number of known Mira variables increased to 251 between 1796 and 1896 (Hoffleit 1997). At the beginning of the twentieth century, more and more Mira-type variables were discovered and their pulsation periods measured (e.g., Hertzsprung 1928; Lause 1930; Kukarkin 1957; Koval 1957; Whitney 1960). After half a century of observations, members of the American Association of Variable Star Observers (AAVSO) collected three million measurements of visual magnitudes of Mira-type variables (Campbell 1955). Along with the technological development, regular observations of Miras in the near-infrared (NIR) passbands began (Lockwood & Wing 1971; Barnes 1973; Whitney 1975; Lloyd Evans 1976; Catchpole et al. 1979; Glass & Feast 1982). At the same time, intensive spectroscopic studies of Mira-type variables were carried out (Keenan 1966; Keenan et al. 1974; Hinkle et al. 1982). Maciel (1976), Wood & Cahn (1977), and Wood (1979) studied the mass-loss phenomenon of Miras, which is still the subject of intense research (e.g., Uttenthaler et al. 2019; Nhung et al. 2022). The NIR period–luminosity relation (PLR) for Miras was first shown by Glass & Lloyd Evans (1981), based on 11 Miras from the Large Magellanic Cloud (LMC).

Mira-type variables could be identified by four fundamental observational properties: their pulsation period, brightness variation amplitude, color index, and shape of light curve. Miras are fundamental-mode pulsators, with periods ranging from about 80 days to over 1000 days. Recently, Trabucchi & Mowlavi (2022) presented an analysis of the period–age relation for LPVs, including Miras. The authors showed that the pulsation period (of the fundamental mode; in general, other LPVs can pulsate in more than one mode) decreases with increasing age, because of the dominant role of mass in shaping the stellar structure and evolution.

Miras show large brightness variations, which are larger at short wavelengths (the peak-to-peak amplitudes in the *V*-band

Original content from this work may be used under the terms of the Creative Commons Attribution 4.0 licence. Any further distribution of this work must maintain attribution to the author(s) and the title of the work, journal citation and DOI.

are higher than 2.5 mag; Samus' et al. 2017), and decrease toward the infrared part of the light spectrum (above 0.4 mag in the *K*-band; Whitelock et al. 2006; Ita et al. 2021; Iwanek et al. 2021b). Mira-type variables with the lowest brightness amplitudes smoothly turn into another LPV subgroup—semiregular variables (SRVs). Miras and SRVs are customarily separated by amplitude, and stars with an *I*-band amplitude greater than 0.8 mag are classified as Mira-type (Soszyński et al. 2009, 2013). This boundary is conventional, and misclassifications are possible around the *I*-band amplitude of 0.8 mag. Miras (and other LPVs) are divided into oxygen-rich (O-rich) and carbon-rich (C-rich) classes, depending on their surface composition and C/O ratio (e.g., Riebel et al. 2010). Usually, C-rich Miras clearly change their mean magnitude over time, while O-rich Miras usually do not show long-term irregular light variations. This is caused by the mass-loss phenomenon and the strong influence of circumstellar dust on stellar light (Iwanek et al. 2021b; Ou & Ngeow 2022).

A relatively short stage in a star's life, the Mira phase is characterized by large bolometric luminosities (ranging from several hundred to tens of thousands of the solar luminosity; Iwanek et al. 2021b) and low average densities (about 7–8 orders of magnitude lower than the solar density; Berlioz-Arthaud 2003; Catelan & Smith 2015). High-amplitude pulsations cause mass-loss phenomena via the stellar wind (Perrin et al. 2020), which leads to the enrichment of the interstellar medium with elements heavier than nickel produced by the slow neutron-capture process. Therefore, Miras, like other LPVs, are important tracers of galactic chemistry (Whitelock et al. 1997; Battistini & Bensby 2016; Kraemer et al. 2019; Yu et al. 2021).

Due to the large brightness and well-defined PLRs in NIR and mid-infrared (mid-IR) wavelengths (Ita & Matsunaga 2011; Yuan et al. 2018; Bhardwaj et al. 2019; Groenewegen et al. 2020), Mira-type stars are promising distance indicators, and a suitable tool for studying stellar populations and structures of galaxies (Soszyński et al. 2009, 2011; Whitelock et al. 2013; Whitelock & Feast 2014; Menzies et al. 2015; Yuan et al. 2017; Whitelock et al. 2018; Huang et al. 2018; Menzies et al. 2019; Huang et al. 2020; Grady et al. 2020; Urago et al. 2020).

Recently, Iwanek et al. (2021a) calibrated PLRs in seven mid-IR bands from the Wide-field Infrared Survey Explorer and Spitzer Space Telescope (wavelengths from 3.4 μm to 22 μm), for the O-rich and C-rich Miras separately. These PLRs allow the measuring of the distance to a single Mira with precision at the level of 5%. On the other hand, Iwanek et al. (2021b) provided synthetic PLRs in 42 bands of existing and future sky surveys, including, e.g., the James Webb Space Telescope, the Nancy Grace Roman Space Telescope (formerly WFIRST), the Vera C. Rubin Observatory (formerly LSST), the Hubble Space Telescope, or the VISTA Near-Infrared YJK_s Survey of the Magellanic Cloud System.

The growing number of known Miras—and therefore the ability to use them to study the structures of galaxies and population properties—has been possible thanks to large-scale surveys providing multiband time-series photometry or spectroscopy of variable stars. Among the various sky surveys, one can distinguish, e.g., the Asteroid Terrestrial-impact Last Alert System (Heinze et al. 2018), the All Sky Automated Survey (ASAS; Pojmański 1997), the All-Sky Automated Survey for Supernovae (ASAS-SN; Shappee et al. 2014; Jayasinghe et al. 2019), the Catalina Sky Survey (Drake et al. 2014, 2017), Gaia (Gaia Collaboration et al. 2016, 2018; Mowlavi et al. 2018), the Kilodegree Extremely Little Telescope (Pepper et al. 2007; Arnold et al. 2020), the Large Sky Area Multi-Object Fiber Spectroscopic Telescope (Yao et al. 2017), the MAssive Compact Halo Objects (Alcock et al. 1995; Bernhard & Hümmerich 2013), the Panoramic Survey Telescope and Rapid Response System (Chambers et al. 2016; Flewelling et al. 2020), the VISTA Variables in the Via Lactea (Minniti et al. 2010), the Zwicky Transient Facility (ZTF; Bellm et al. 2019; Chen et al. 2020), and, finally, the Optical Gravitational Lensing Experiment (OGLE; Soszyński et al. 2013; Udalski et al. 2015).

This paper focuses on almost 66,000 Mira-type stars found in the OGLE databases in the Galactic bulge (BLG) and Galactic disk (GD) fields. In the International Variable Star Index (VSX; Watson et al. 2006),[3] over 28,000 variable stars are classified as Mira from the entire sky (type M). The vast majority of the objects presented in this paper are new discoveries, which have been possible thanks to the two-decade-long well-sampled high-quality time-series OGLE photometry. With this catalog, we triple the number of known Miras in the Milky Way. This collection of Miras will be part of a much larger collection of LPVs found in the Galaxy, which will be a supplement to the LPV collections found toward the BLG in the OGLE-III database (Soszyński et al. 2013).

The paper is organized as follows. In Section 2, we describe the photometric data used in the analysis. In Section 3, we discuss our methods for the selection and classification of Mira stars, but we also describe the method of the period search and the measurement of the mean magnitudes and variability amplitudes. Section 4 presents the structure of the collection. In Section 5, we discuss the statistical properties of Mira-type variable stars in the BLG and GD. The paper is summarized in Section 6. The long-term two-band time-series photometry, together with finding charts for all stars, are available from the OGLE Internet Archive.[4]

2. Observations and Photometric Data

The OGLE project is one of the longest-lasting variability sky surveys worldwide. Historically, the first OGLE observations were taken in 1992, using the 1.0 m Swope Telescope located at the Las Campanas Observatory, Chile (the OGLE-I phase; Udalski et al. 1992). The observatory is operated by the Carnegie Institution for Science. The second phase of the OGLE survey (OGLE-II) started in 1997, at the Las Campanas Observatory, with the new 1.3 m Warsaw Telescope dedicated to the project (Udalski et al. 1997). Since then, regular monitoring of the BLG, GD, and Magellanic Clouds has been carried out. During the two decades until 2020, the OGLE project went through two more phases: OGLE-III (2001–2009; Udalski 2003) and OGLE-IV (2010–2020; Udalski et al. 2015). Between these phases, the CCD camera was upgraded, filling the entire 1.4 square degree field of view of the Warsaw Telescope in the OGLE-IV phase, with the pixel scale equal to 0.″26. The two-decade-long monitoring of the southern sky was suspended in 2020 March due to the COVID-19 pandemic. Therefore, the last epoch in the collection was taken during the night of 2020 March 17/18.

[3] https://www.aavso.org/vsx/ (as of 2022 March 30).
[4] https://www.astrouw.edu.pl/ogle/

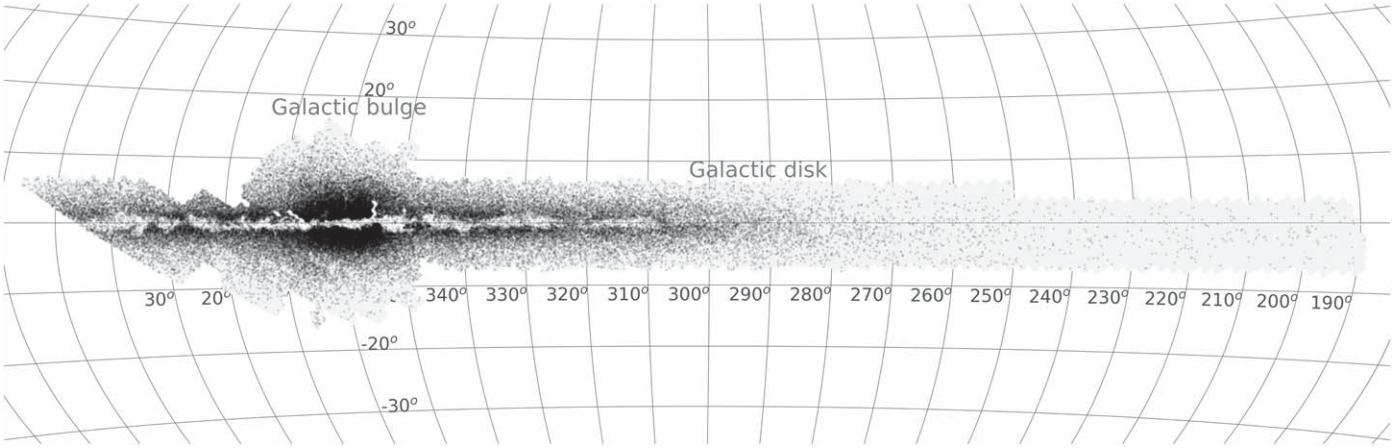

Figure 1. Distribution of Miras (black points) in the Galactic coordinates. Our catalog contains 40,356 Mira-type variables in the BLG and 25,625 in the GD. The gray area shows the OGLE-IV footprint of the Milky Way.

The OGLE observations were carried out in the Johnson *V*-band (mean wavelength of 0.55 μm) and Cousins *I*-band (mean wavelength of 0.81 μm) filters. The vast majority of the photometric data were obtained in the *I*-band. Currently, less than half of all stars observed by the OGLE survey have any *V*-band observations. The exposure time in the *I*-band for the GD and outer BLG fields (the outer parts of the BLG) was 25 s, while the typical exposure time in the BLG fields was 100 s (mostly the inner parts of the BLG). The magnitude range in the GD and outer BLG fields is a little wider than in the standard BLG survey, spanning from 10 mag to 20 mag, in contrast to the BLG fields with an exposure time of 100 s, where the magnitudes span from 13.5 mag to 21.5 mag. Observations in the *V*-band were taken less frequently, most often for the purpose of determining the $(V-I)$ color indices of stars. Therefore, the number of epochs in the *V*-band is on average an order of magnitude smaller than in the *I*-band. The exposure time in the *V*-band for the GD and outer BLG fields was 25 s, while for the inner BLG observations it was 150 s. For *I*-band magnitudes brighter than 15 mag, the uncertainty of a single photometric measurement is smaller than 0.01 mag, with a typical value of 0.005 mag, while stars with magnitudes ranging between 15 mag and 18 mag have photometric uncertainties smaller than 0.05 mag. In the *V*-band, stars brighter than 18 mag have photometric uncertainties smaller than 0.01 mag, with a typical value of 0.005 mag. In total, the OGLE-IV survey covers ∼3000 square degrees of the sky. The OGLE-IV footprint of the Milky Way is presented in Figure 1.

The OGLE project uses difference image analysis (DIA; Alard & Lupton 1998; Woźniak 2000) to obtain photometry of the sources. For more information about the technical details, instrumentation, data processing, sky coverage, or calibration in each OGLE phase, we encourage the reader to see the papers by Udalski et al. (1992, 1997), Udalski (2003), and Udalski et al. (2008, 2015).

3. Selection and Classification of Miras

To date, only one catalog of LPVs toward the BLG has been published, based on the OGLE-III data (Soszyński et al. 2013). Among ∼230,000 LPVs, the authors found 6528 Mira-type variables. The vast majority of the sample consists of the OGLE small-amplitude red giants (over 190,000 objects). A search for LPVs in the GD fields has never been carried out based on the OGLE data, but 31 LPVs were found during an analysis of an OGLE-III GD area of 7.12 square degrees in the direction tangential to the Centaurus Arm (Pietrukowicz et al. 2013).

In this paper, we are interested in finding Mira-type variable stars. Mira variability is characterized by a large brightness amplitude (conventionally equal to or greater than 0.8 mag in the *I*-band; Soszyński et al. 2013) and long pulsation periods (from about 80 days to more than 1000 days). Moreover, Miras pulsate solely in the fundamental mode, so a single significant period is expected.

The search for Miras began by selecting over a billion point sources in the BLG and GD fields, from which we excluded the already classified and published Miras (Soszyński et al. 2013; Pietrukowicz et al. 2013). In the second step, we subtracted long-term trends estimated with cubic splines from the *I*-band OGLE-IV light curves to properly determine the amplitude of the brightness variations. After that, we calculated the *I*-band brightness amplitude, defined as the difference between the faintest and brightest data points, rejecting 2.5% of points from both sides of the brightness distribution to avoid amplitude contamination by outlying measurements. Then, we measured the change of dynamics in the brightness between the closest consecutive measurements, given by the equation

$$c = \frac{A_I}{\frac{1}{n}\sum_{i=1}^{n-1}\frac{|\,I(t_{i+1})-I(t_i)\,|}{t_{i+1}-t_i}}, \quad (1)$$

where A_I is the *I*-band brightness amplitude, $I(t_{i+1})$ and $I(t_i)$ are the *I*-band brightness of two consecutive measurements, and $t_{i+1}-t_i$ is the time difference between these measurements. This coefficient was calculated using all n points of light curves, taking into account only those pairs of measurements for which the time difference was smaller than 10 days (i.e., $(t_{i+1}-t_i)<10$ d). The larger the coefficient c, the greater the probability that the analyzed star is of the Mira type (or an LPV in general). We randomly selected several dozen light curves from many different ranges of this coefficient and visually inspected each of them. We noticed that if the coefficient c was below 15 days, we no longer detected Miras in the sample. Out of all the light curves, we accepted those with a coefficient c greater than or equal to 15 days only. This limit was chosen experimentally, and it is arbitrary. Moreover, we made an amplitude cut, and we removed all objects

with a brightness amplitude below 0.5 mag. This left us with 194,522 light curves for further analyses.

For the selected light curves, we calculated periods using two methods: the Lomb–Scargle periodogram (LS; Lomb 1976; Scargle 1982; VanderPlas 2018) and the FNPEAKS code[5] (created by Z. Kołaczkowski, W. Hebisch, and G. Kopacki, 2003), based on the standard discrete Fourier transform modified for unevenly spaced data (Kurtz 1985). A detailed discussion of the period searching methods for such data can be found in Iwanek et al. (2019).

We searched the frequency space from 0.0005 to 0.1 day^{-1} (periods from 10 to 2000 days), with a resolution of 10^{-6} day^{-1}. At this stage of the analysis, the most arduous and lengthy process began, i.e., the visual inspection and classification of the stars. The selection and classification processes, based on the visual inspection of light curves by experienced astronomers, guarantee the high purity and completeness of our catalogs. Our priority is to find all objects of a given type in the OGLE databases, while, at the same time, making sure not to contaminate the sample with other types of variability.

We checked by eye both raw (unfolded) and folded light curves. The light curves of the stars classified as Miras were checked after being folded against each of the measured periods (from the FNPEAKS and LS methods). If both periods were similar, we chose the one that phased the light curve better, i.e., gave a smaller scatter of points. If one of the periods was correct, we left it without any changes. In the case when both periods were incorrect, we corrected the period manually. In this step, we also removed any obvious outlying measurements. Here, we classified 60,997 stars as Mira candidates. More than half of the examined light curves were classified as artifacts, e.g., caused by bright, saturated stars. We also found a few thousand SRVs, a few thousand stars with other variability types, a few hundred long secondary period variables (see, e.g., Soszyński et al. 2021), and, finally, several microlensing events.

Some OGLE fields partially overlap, so stars located on the edges of the fields are measured twice, and have more than one light curve in our database. Such pairs of stars could be used to estimate the completeness of the catalog (for a detailed description, see Section 4.1). We found 2630 pairs of stars in the overlapping areas of adjacent OGLE fields. Typically, stars in these pairs differ in the number of measurements and the quality of measurements (i.e., measurement uncertainties). We visually inspected each pair, and we chose that element of the pair that had a better light curve in the sense of its measurement uncertainties and its number of data points. After that, the number of Mira candidates dropped to 58,367.

3.1. Determination of Final Periods, Mean Magnitudes, and Amplitudes

The periods measured for stars classified as Miras, although manually corrected and verified by eye, may still be inaccurate. We decided to fine-tune periods by using the TATRY code, which implements multiharmonic analysis of the variance algorithm (Schwarzenberg-Czerny 1996). We did not use the TATRY code for the initial period determination, because this method requires more computational time compared to the ones we did use. For most stars, the period found in this way was very close to that accepted during the visual inspection of the light curves. In such cases, we chose this period as the final one. However, in some cases, the differences between the periods were significant. Therefore, we verified the light curves phase-folded with both periods, and applied the period that phased the light curve best. For period fine-tuning, we used all the available OGLE data.

After the pulsation period fine-tuning, we decided to fine-tune the brightness variation amplitude. We phase-folded each light curve with the best period. As OGLE light curves may be unevenly sampled, we filled the gaps between the data points using cubic spline interpolation. Then, we fitted a third-order truncated Fourier series, using the measured period to the phase-folded "filled" light curve, and we measured the peak-to-peak amplitude. A similar procedure was applied to the mean magnitude measurements, with the difference that we fitted the third-order Fourier series to a light curve transformed to the flux scale. We integrated the fit to determine the mean brightness, and, finally, we transformed the mean brightness to the magnitude scale. The *I*-band amplitude and both the *I*- and *V*-band mean magnitudes were measured based on the OGLE-IV data. In the case that data from the fourth phase of the OGLE project were not available, the measurements were made using data from the previous phases of the survey.

3.2. Amplitude Cut

Soszyński et al. (2013) adopted an *I*-band amplitude division line between SRVs and Miras equal to 0.8 mag (see Figure 8 therein). We adopted the same division value, to remove stars with *I*-band amplitudes smaller than 0.8 mag. This step left us with 58,047 Mira-type variable stars. The removed stars were classified as SRVs, and will be published in the full version of the OGLE collection of LPVs.

This amplitude limit is conventional, and stars with amplitudes close to 0.8 mag may be misclassified. On the other hand, we found stars that change amplitudes, and their classifications change over time, from Miras to SRVs and vice versa. Such cases are described in Section 3.3.

3.3. Reexamining the OGLE-III Catalog

In the OGLE-III catalog of LPVs toward the BLG, Soszyński et al. (2013) classified 6528 stars as Mira-type. We reexamined all these stars based on the OGLE-IV light curves. We applied the methods described in Sections 3.1 and 3.2, and we visually inspected all these light curves. We found that the amplitudes of 112 stars were changing over time and were fluctuating around 0.8 mag. For such stars, we decided to change their classification from Miras to SRVs, and we excluded them from the sample. In Figure 2, we present two examples of stars that change their brightness variation amplitude significantly over time, thus the classification of such stars is not obvious. Stars "switching" between Mira-type and SRVs are important from the evolutionary point of view, because SRVs are believed to be the progenitors of Miras (e.g., Trabucchi & Mowlavi 2022), so they should be examined in detail.

Consequently, we were left with 6416 Miras from the OGLE-III catalog (Soszyński et al. 2013), and we supplemented our sample with these stars. The number of Miras increased to 64,463.

3.4. Crossmatching with Other Catalogs of Variable Stars

We crossmatched our sample with the VSX (Watson et al. 2006),[6] the ASAS-SN variable stars catalog (Shappee et al. 2014; Jayasinghe et al. 2019), and the ZTF variable stars

[5] http://helas.astro.uni.wroc.pl/deliverables.php?active=fnpeaks

[6] https://www.aavso.org/vsx/index.php

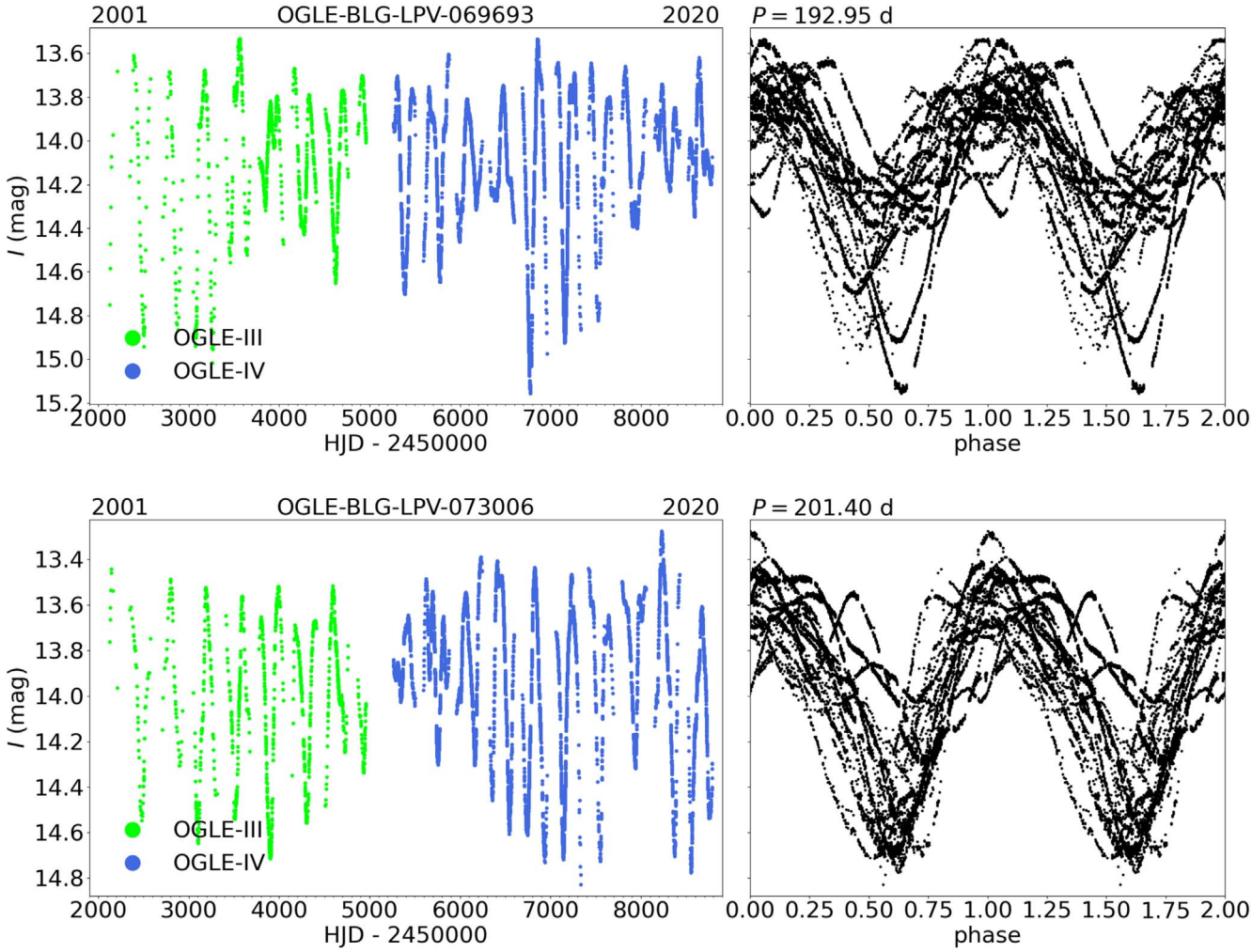

Figure 2. Two examples of stars that were classified as Miras by Soszyński et al. (2013), but whose amplitudes change significantly over time and fluctuate around 0.8 mag. Such stars were reclassified from Miras to SRVs and excluded from the sample. The left-hand-side panels show unfolded light curves, while the right-hand-side panels show phase-folded light curves with pulsation periods P (provided above the plots). The dates at the tops of the unfolded light curves mark the years when the observations started and the year of the last used observations. The individual phases of the OGLE project are marked with different colors.

catalog (Bellm et al. 2019; Chen et al. 2020). We checked how many stars from these sources are in the OGLE fields, but were not found during our search. We identified 3275 such objects. We searched the OGLE databases for objects in a radius of $1'$ around the coordinates from the abovementioned catalogs. We extracted all available light curves, measured the pulsation periods and amplitudes for these stars (as described in Section 3.1), and carefully checked each of them. As a result, we supplemented our catalog with 1518 missed Miras, finally closing our search for Mira-type variables in the Milky Way. The remaining 1757 stars turned out to be variables of other types (mainly SRVs), were too bright to be observed by the OGLE survey, or did not have a counterpart in the OGLE database, probably due to inaccurate coordinates being provided in the external catalogs. In total, our collection consists of 65,981 Mira variables. The distribution of Miras in the sky is presented in Figure 1.

4. The OGLE Collection of Mira Variables

We present the OGLE collection of Mira stars in the Milky Way, which contains 65,981 objects in total. This is the largest, purest, and most complete catalog of Mira-type variables to date. The data for all these stars are available through the OGLE website and file transfer protocol (FTP):

1. https://www.astrouw.edu.pl/ogle/ogle4/OCVS/blg/lpv/—objects in the BLG fields.
2. https://www.astrouw.edu.pl/ogle/ogle4/OCVS/gd/lpv/—objects in the GD fields.
3. ftp.astrouw.edu.pl/ogle/—FTP for the entire OGLE Collection of Variable Stars.
4. https://ogledb.astrouw.edu.pl/~ogle/OCVS/—user-friendly search engine for the entire OGLE Collection of Variable Stars.

Each object has an individual identifier: OGLE-BLG-LPV-NNNNNN or OGLE-GD-LPV-NNNNNN, where NNNNNN is a six-digit number. The identifiers of the stars in the BLG fields remain unchanged with respect to the collection published by Soszyński et al. (2013). Stars discovered in the OGLE-IV data receive new identifiers, and are listed in an ascending R.A. order. To date, only 31 LPVs (18 Miras and 13 SRVs) from the GD area have been discovered in the OGLE data (Pietrukowicz et al. 2013). Our collection of Miras contains 20 objects from the Pietrukowicz et al. (2013) catalog (two stars previously categorized as SRVs have been reclassified as Miras). Their

Table 1
Table `ident.dat` with Identifications and Equatorial Coordinates for All Miras

ID	Type	Loc.	R.A. (h:m:s)	Decl. (deg:m:s)	OGLE-IV ID	OGLE-III ID	OGLE-II ID	Other ID
OGLE-BLG-LPV-000009	Mira	BLG	17:05:28.47	−32:44:22.4	BLG897.03.15	BLG366.6.6796	—	Terz V 3396
OGLE-BLG-LPV-000018	Mira	BLG	17:05:37.00	−33:02:36.6	BLG898.27.195	BLG366.8.10859	—	—
OGLE-BLG-LPV-000024	Mira	BLG	17:05:43.89	−33:02:32.6	BLG898.27.79	BLG366.8.10875	—	—
OGLE-BLG-LPV-000028	Mira	BLG	17:05:52.29	−32:39:49.4	BLG897.02.55701	BLG366.6.69850	—	—
OGLE-BLG-LPV-000030	Mira	BLG	17:05:55.21	−32:50:24.6	BLG898.27.60162	BLG366.7.42260	—	Terz V 3407
OGLE-BLG-LPV-000092	Mira	BLG	17:07:36.82	−32:48:40.3	BLG908.16.54571	BLG366.2.82751	—	Terz V 3484
OGLE-BLG-LPV-000106	Mira	BLG	17:07:44.70	−32:30:20.8	BLG908.24.58094	BLG366.4.89376	—	Terz V 3493
OGLE-BLG-LPV-000113	Mira	BLG	17:07:50.52	−32:43:04.1	BLG908.24.73	BLG366.3.26435	—	Terz V 3498
OGLE-BLG-LPV-000142	Mira	BLG	17:08:39.85	−32:58:09.9	BLG908.14.267	BLG332.6.12	—	—
OGLE-BLG-LPV-000147	Mira	BLG	17:08:40.98	−32:54:57.2	BLG908.14.58864	BLG332.6.61774	—	Terz V 3538
OGLE-GD-LPV-025636	Mira	GD	19:16:07.04	−00:06:14.3	DG1071.17.12320	—	—	ASASSN-V J191607.04-000614.3

Note. For each star, we provide its unique ID, variability type (the same for each object; the Mira collection will be part of a much larger collection of LPVs in the Milky Way), J2000 equatorial coordinates, OGLE-IV, OGLE-III, and OGLE-II identifiers, and also identifiers from other catalogs (the best matches), i.e., the VSX/ASAS-SN/ZTF catalogs. The "–" sign means a lack of a match with other databases.

(This table is available in its entirety in machine-readable form.)

Table 2
Table `Miras.dat` with Observational Parameters of Each Star: the *I*- and *V*-band Mean Magnitudes, Pulsation Period, and the *I*-band Amplitude

ID	Loc.	I (mag)	V (mag)	P (days)	A_I (mag)
OGLE-BLG-LPV-000009	BLG	13.008	—	275.3	2.345
OGLE-BLG-LPV-000018	BLG	13.568	—	363.9	2.333
OGLE-BLG-LPV-000024	BLG	12.718	—	245.7	1.848
OGLE-BLG-LPV-000028	BLG	12.868	—	386.8	1.488
OGLE-BLG-LPV-000030	BLG	12.133	—	172.01	1.926
OGLE-BLG-LPV-000092	BLG	12.980	—	348.1	2.145
OGLE-BLG-LPV-000106	BLG	13.051	—	363.1	2.764
OGLE-BLG-LPV-000113	BLG	13.315	—	342.1	1.428
OGLE-BLG-LPV-000142	BLG	13.190	—	268.1	2.626
OGLE-BLG-LPV-000147	BLG	12.493	—	208.1	1.774
OGLE-GD-LPV-025636	GD	12.207	—	255.5	3.257

Note. For each star, we provide the *I*-band and *V*-band (if available; in total, *V*-band light curves are available for 19,779 stars) mean magnitudes, pulsation period, and the *I*-band amplitude. The "–" sign for the *V*-band mean magnitude means that the *V*-band light curve is not available.

(This table is available in its entirety in machine-readable form.)

Table 3
The Median (Med.) and Maximum (Max.) Number of Epochs in the Light Curves, Separately for Each OGLE Phase, and with Division into Locations and Bands

Phase	Band	Location	Med.	Max.	% of Miras
OGLE-II			310	550	4%
OGLE-III	*I*	BLG	623	2532	15%
OGLE-IV			227	16,686	97%
OGLE-II			9	18	3%
OGLE-III	*V*	BLG	5	41	10%
OGLE-IV			42	230	27%
OGLE-II			125	553	1%
OGLE-III	*I*	GD	1676	2696	0.1%
OGLE-IV			130	1307	99%
OGLE-II			69	98	0.01%
OGLE-III	*V*	GD	4	8	0.06%
OGLE-IV			8	16	30%

Note. We also provide the fraction of Miras that have light curves in the indicated OGLE phases and bands, relative to the total number of Miras in the BLG (40,356 stars) and GD fields (25,625 stars).

designations are the same as in the OGLE-III catalog, but we have increased the number of digits in the identifiers from four to six. In the future, we plan to publish a much larger collection of LPVs in the Milky Way, of which this collection of Mira stars will be a part.

The websites of the OGLE collection of Miras are structured as follows. The file `ident.dat` contains the list of stars with their classifications, J2000 equatorial coordinates, identifications in the OGLE-II, OGLE-III, and OGLE-IV databases, and designations taken from the VSX/ASAS-SN/ZTF catalogs (in total, we identified 12,033 Miras in external catalogs of variable stars). The identifiers of the Miras in the OGLE databases contain shortcuts for the OGLE fields, identifying the positions of the stars in the sky: BLG is for stars located in the inner and outer Galactic bulge fields, GD is for stars located in the Galactic disk fields with a negative Galactic longitude, and DG is for stars located in the Galactic disk fields with a positive Galactic longitude. In the file `Miras.dat`, we provide observational parameters for each star—the pulsation period, mean magnitudes in the *I*- and *V*-bands, and *I*-band brightness amplitude. The files `ident.dat` and `Miras.dat` are also provided with this paper in a machine-readable form (merged for both environments). In Tables 1 and 2, we present the first ten rows plus the last row from the tables `ident.dat` and `Miras.dat`, for guidance regarding their form and content.

The subdirectory `fcharts/` contains finding charts for all objects. We provide $60'' \times 60''$ subframes of the *I*-band DIA reference images, oriented with north up, and east to the left. The object is marked with a white cross and is in the center of the frame.

In the subdirectories `phot_ogle2/`, `phot_ogle3/`, and `phot_ogle4/`, we provide the *I*-band and *V*-band (if available) time-series photometry from the OGLE-II (1997–2000), OGLE-III (2001–2009), and OGLE-IV (2010–2020) phases, respectively. All available data from the OGLE photometric databases are included here. The data from different phases were calibrated separately to the standard Johnson–Cousins photometric system. During our classification, we removed any obvious outlying points from the light curves. We encourage the reader to pay attention to possible offsets between photometric zero-points for the light curves obtained during different phases of the OGLE project. The typical uncertainties of the OGLE photometric calibrations do not exceed 0.05 mag, but in individual cases, much larger offsets may occur, which can be a result of several factors, e.g., high local star density, which causes blending. Therefore, significant offsets should be taken into account during the light curve merging process (if needed).

The *I*-band light curves (from at least one of the OGLE phases) are available for all of the Mira stars in our collection. In turn, the *V*-band observations are available only for 19,779 stars (11,883 from BLG and 7896 from GD). The epoch number statistics of the OGLE light curves, separately for BLG and GD, and with a division into *I*-band and *V*-band, are presented in Table 3. In Figures 3 and 4, we present three examples of Miras observed in the BLG (Figure 3) and GD fields (Figure 4). Each figure moves from presenting a light curve that is well-covered (the largest number of measurements, top panel) to one that is poorly covered (bottom panel). In these figures, we also present finding charts for each star.

Our collection includes 939 Miras observed continuously from 1997, i.e., from the beginning of the OGLE-II phase, until 2020 March, when the telescope had to be closed due to the COVID-19 pandemic. This data set contains objects that significantly change their mean magnitudes or brightness amplitudes over time, or whose pulsation period lengthens or shortens. This is a unique data set that can be used to study, e.g., the evolution of Miras or the mass-loss phenomenon. Examples of 42 light curves of such objects are presented in Figures 5, 6, and 7.

4.1. Completeness and Purity of the Catalog

The completeness of our collection of Mira variables strongly depends on many factors, e.g., the observed brightness of the stars, the distance to the stars, the interstellar extinction toward the stars, the stability of the light curves, the number of epochs, and the time span of the observations. Unlike other types of variable stars, the amplitudes of the light curves do not limit the completeness of the Mira catalogs, since even the minimum amplitude of 0.8 mag (in the *I*-band) is much larger

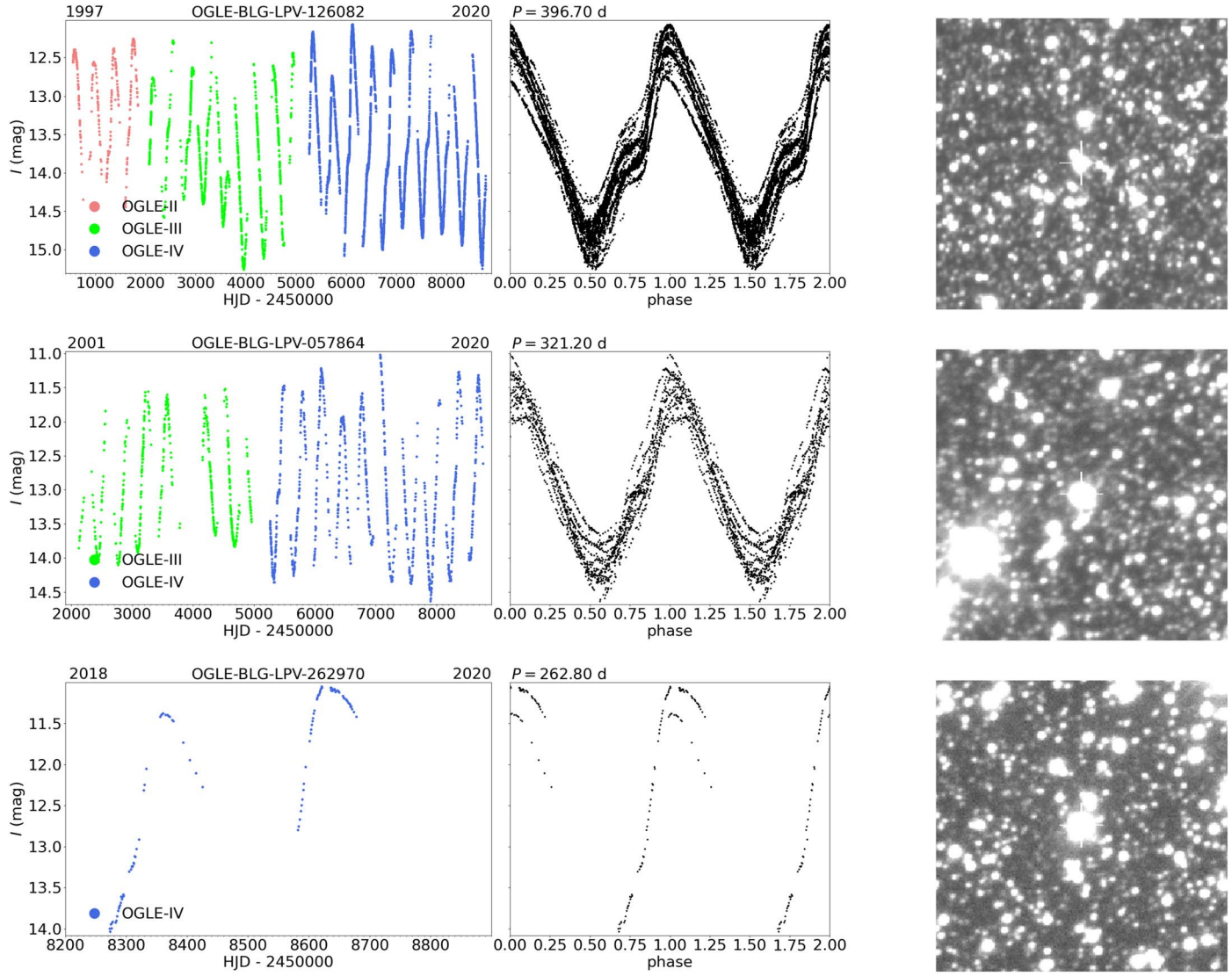

Figure 3. Three examples of Miras from our collection, observed in the BLG fields, with light curves containing a different number of epochs. Top row: a well-covered light curve of Mira OGLE-BLG-LPV-126082. The observations consist of 19,169 epochs that span 23 yr (from 1997 to 2020). Middle row: a medium-covered light curve of Mira OGLE-BLG-LPV-057864. The observations consist of 1593 epochs that span 19 yr (from 2001 to 2020). Bottom row: a poorly covered light curve of Mira OGLE-BLG-LPV-262970. The observations consist of 119 epochs that span 2 yr (from 2018 to 2020). The left-hand-side panels show unfolded light curves, while the right-hand-side panels show phase-folded light curves with pulsation periods P (provided above the plots). The dates at the tops of the unfolded light curves mark the year when the observations started and the year of the last used observations. The phases of the OGLE project are marked with different colors (red, green, and blue). For each star, we also provide the $60'' \times 60''$ finding chart, oriented with north up and east to the left. Each Mira is at the center of the finding chart, and is marked with a white cross.

than the photometric uncertainties of the individual data points. On the other hand, the critical factors in the completeness of the catalog of Miras are the number of epochs and the time span of the observations, as the pulsation periods of Miras are typically longer than 100 days and their light-curve shapes do not repeat precisely from cycle to cycle. During our search for Mira variables, we found several hundred large-amplitude light curves affected by a small number of epochs and a short time span, for which we could not even estimate their periods. Such objects could be also Miras, but we did not have enough evidence to prove it, so we rejected such stars from the sample as we did not want to contaminate the catalog.

We are able to estimate the completeness of our collection using the Miras that have been observed twice by the OGLE survey, because they were located in the overlapping areas of adjacent fields (for more details, see Section 3). Since stars located close to the edges of the fields are usually affected by a smaller number of points, we limited our analysis to pairs of light curves consisting of at least 100 epochs each. Out of the 2630 pairs found, only 1707 pairs met this criterion. Therefore, we had an opportunity to independently detect 3414 counterparts. For 1575 pairs, we successfully identified and classified both Miras, while for the remaining 132 pairs, we detected just one Mira star. This gives the completeness of our collection at a level of 96%.

We carefully checked all of the 132 light curves that we missed during our selection process. Almost all of them were missed because of the small number of epochs, which made it impossible for them to be classified as Miras.

The purity of our collection of Mira stars is limited by the LPVs with amplitudes near the boundary between Miras and SRVs (0.8 mag in the I-band). As described in Section 3.3, and

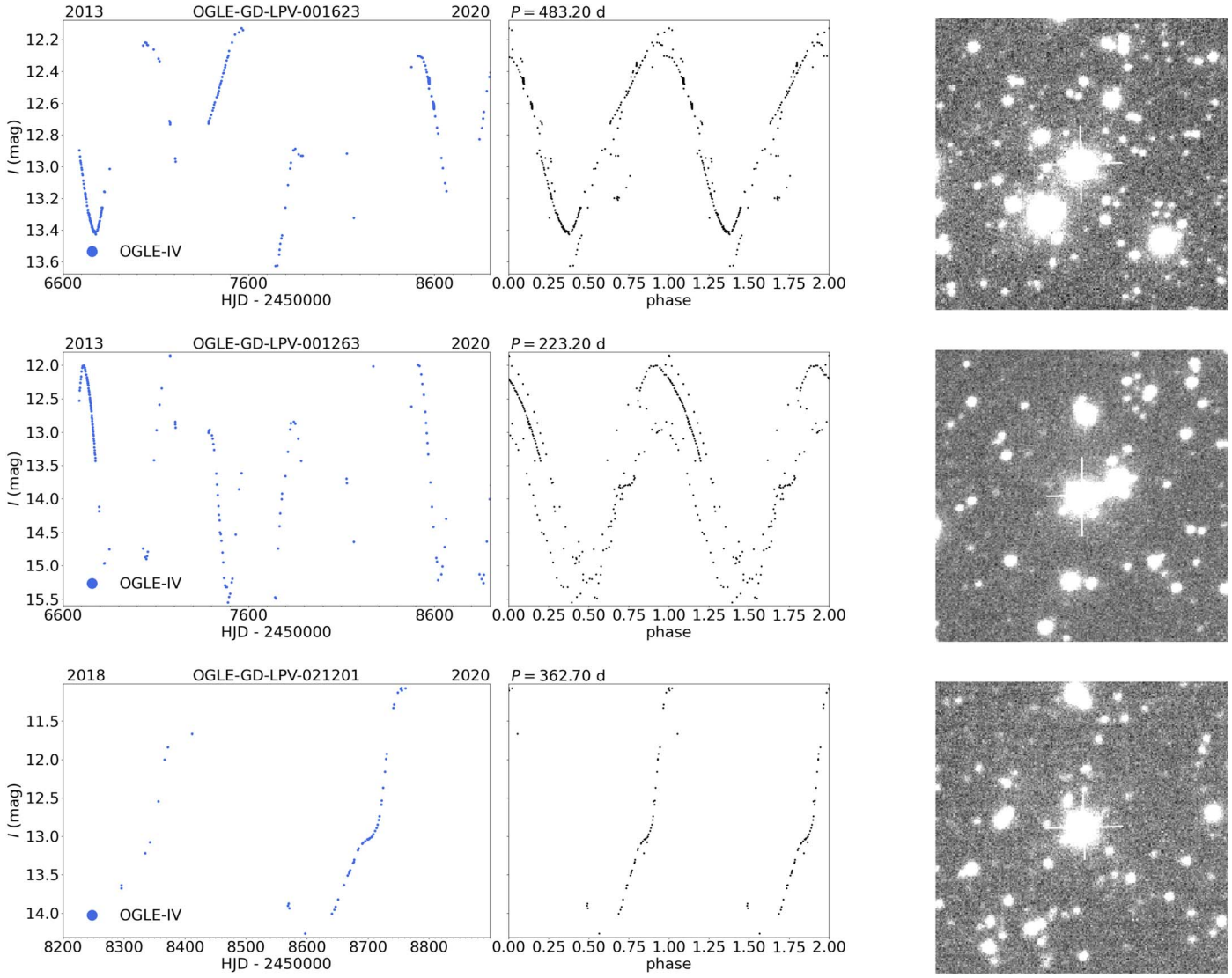

Figure 4. Three examples of Miras from our collection, observed in the GD fields, with light curves containing a different number of epochs. Top row: a well-covered light curve of Mira OGLE-GD-LPV-001623. The observations consist of 1307 epochs that span 7 yr (from 2013 to 2020). Middle row: a medium-covered light curve of Mira OGLE-GD-LPV-001263. The observations consist of 180 epochs that span 7 yr (from 2013 to 2020). Bottom row: a poorly covered light curve of Mira OGLE-GD-LPV-021201. The observations consist of 55 epochs than span 2 yr (from 2018 to 2020). The left-hand-side panels show unfolded light curves, while the right-hand-side panels show phase-folded light curves with pulsation periods P (provided above the plots). The dates at the tops of the unfolded light curves mark the year when the observations started and the year of the last used observations. The fourth phase of the OGLE project is marked with blue. For each star, we also provide the $60'' \times 60''$ finding chart, oriented with north up and east to the left. Each Mira is at the center of the finding chart, and is marked with a white cross.

presented in Figure 2, such stars may oscillate between the Mira and SRV phases. On the other hand, the probability of confusing Mira variables with other types of variable stars (different than LPVs) during the visual inspection of their light curves is very low. As a result, we estimate that the purity of our collection is very high; however, it is unfeasible to give a precise figure.

5. Discussion

In Figure 8, we present histograms of the basic properties of the Miras in our collection, i.e., the I- and V-band magnitudes, the pulsation period, and the I-band brightness amplitude. We show separate histograms for the stars located in the BLG and GD fields.

The distributions of the I-band mean magnitudes (top left panel in Figure 8) are limited on the brighter side of the histograms, which is related to the OGLE saturation limits (see Section 2). The large variability amplitudes enable us to detect Miras brighter than the saturation limit, i.e., we have the opportunity to observe them in phases other than maximum light. The same effect is observed for the faintest Miras, which means that the mean magnitudes are below the detection limit —it is possible to observe these stars around their maximum light and classify them as Miras. Approximately 2% of all the Miras in our collection may be affected by the proximity of their mean brightness to either the saturation or detection limits. For the brightest, as well as the faintest, Miras, their mean magnitudes and brightness amplitudes can be measured with lower accuracy. However, this has the greatest impact for stars with poorly covered light curves. The maxima of the I-band magnitude distributions are similar for the BLG and GD populations, at 13.5 mag for BLG and ∼13.0 mag for GD. The shift in the histogram for the GD population to brighter magnitudes is likely due to the shorter exposure times (so that stars saturate at brighter magnitudes), the shorter distances to these stars, on average, and the lower interstellar extinction.

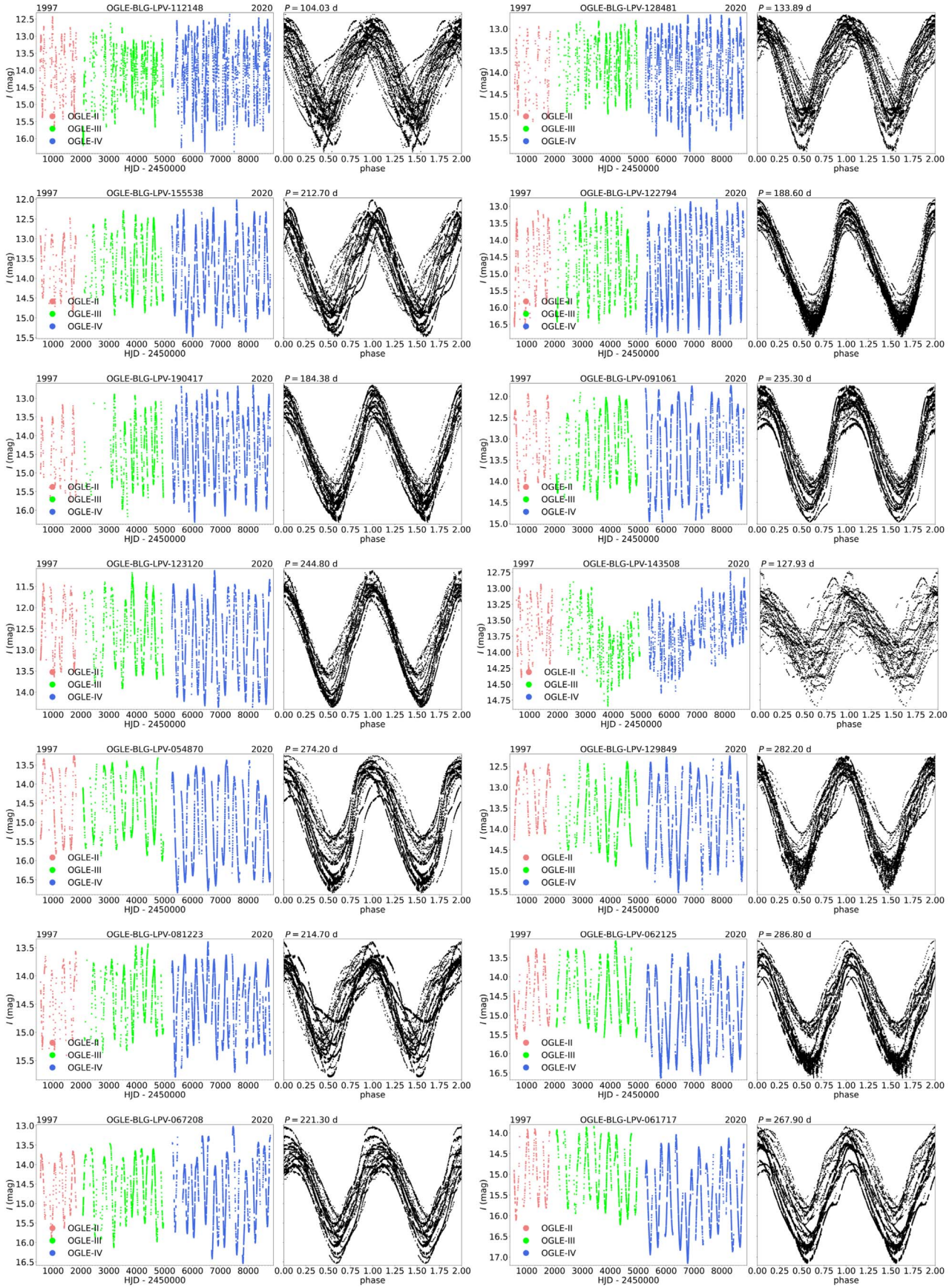

Figure 5. 14 examples of Mira stars from our catalog that were observed from 1997, i.e., the beginning of the OGLE-II phase, until 2020 March. The left-hand-side panels show unfolded light curves, while the right-hand-side panels show phase-folded light curves with pulsation periods P (provided above the plots). The dates at the tops of the unfolded light curves mark the year when the observations started and the year of the last used observations. The individual phases of the OGLE project are marked with different colors (red, green, and blue).

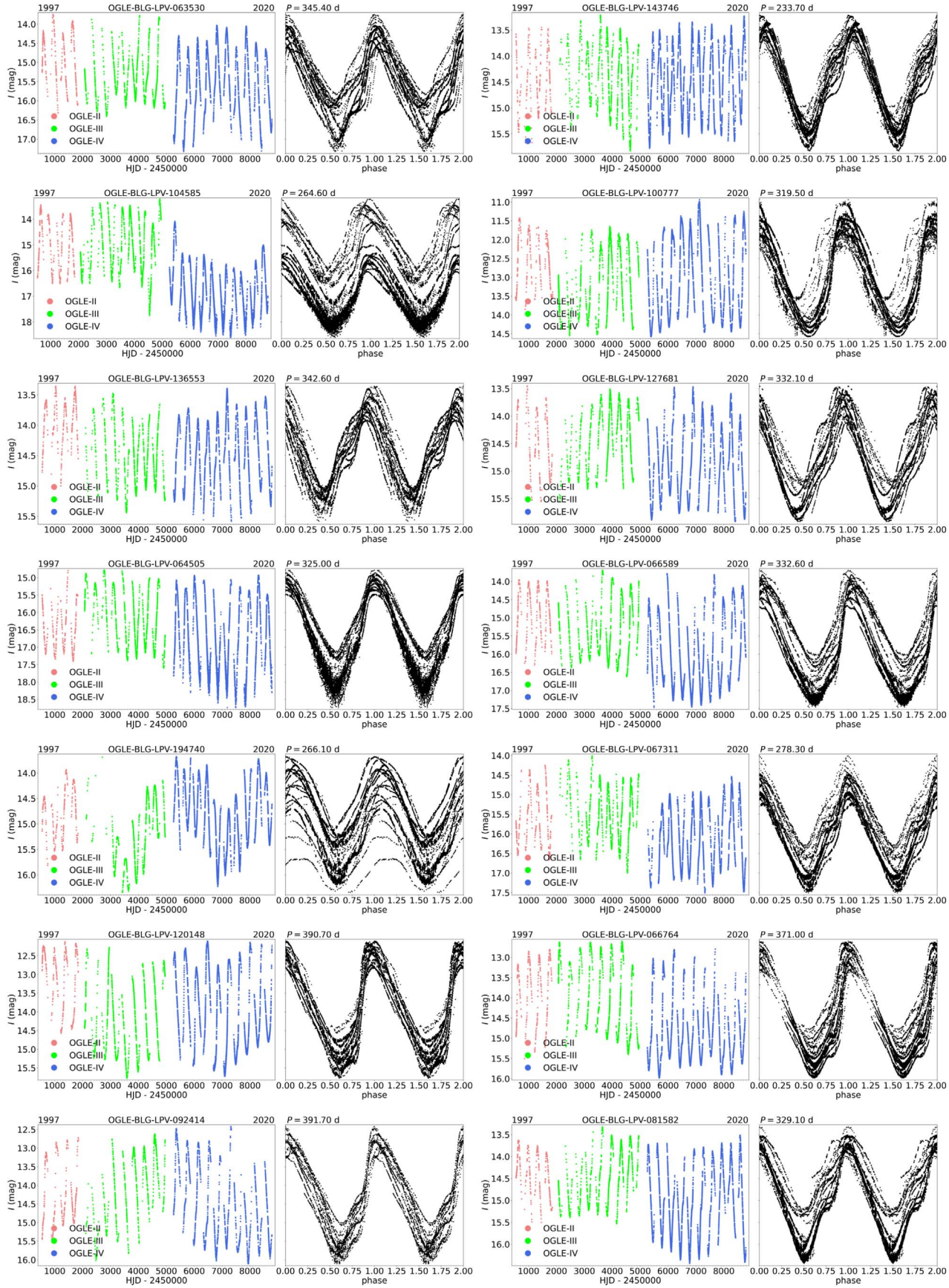

Figure 6. The same as Figure 5, but 14 other Miras are presented.

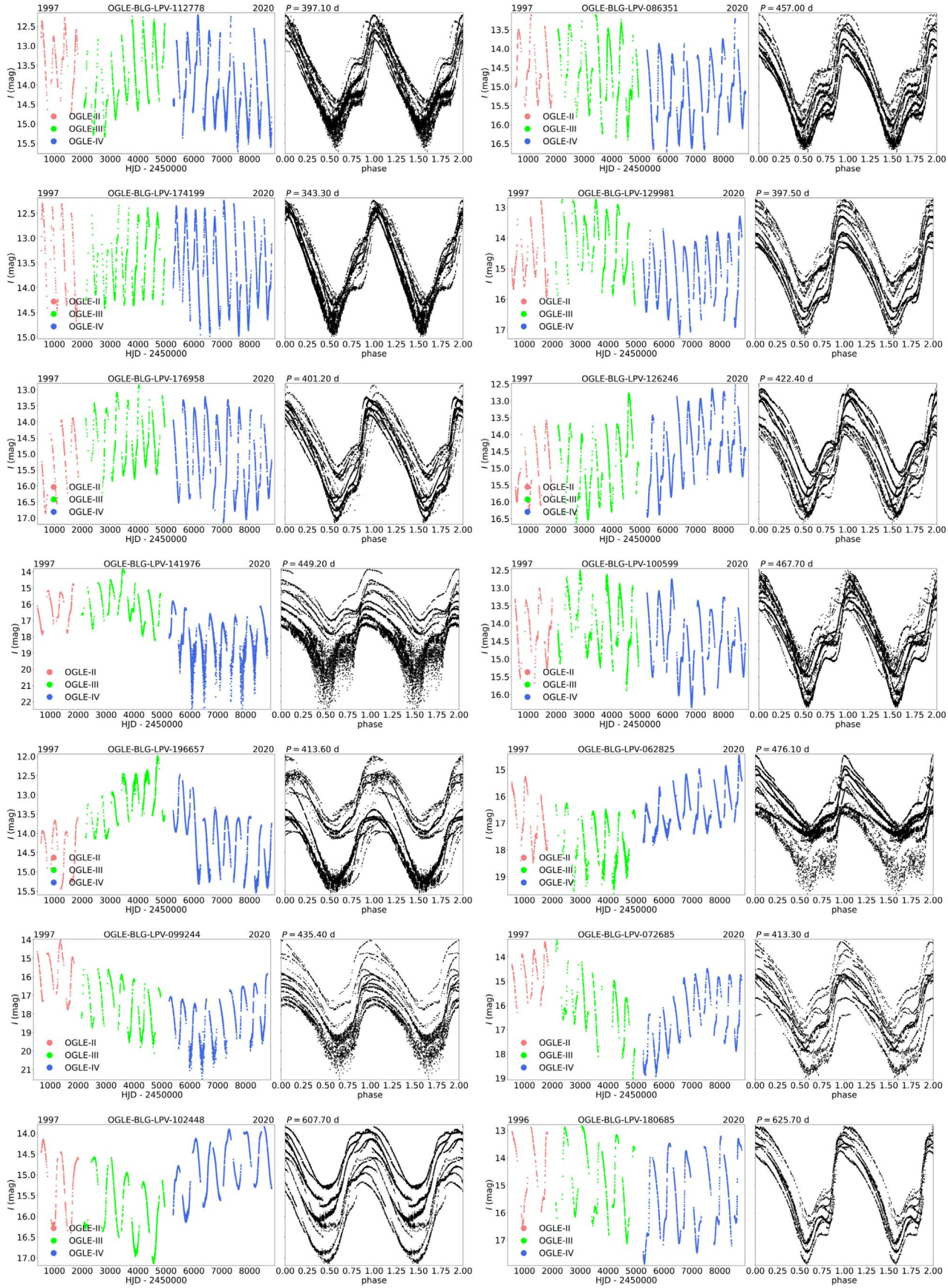

Figure 7. The same as Figures 5 and 6, but 14 other Miras are presented.

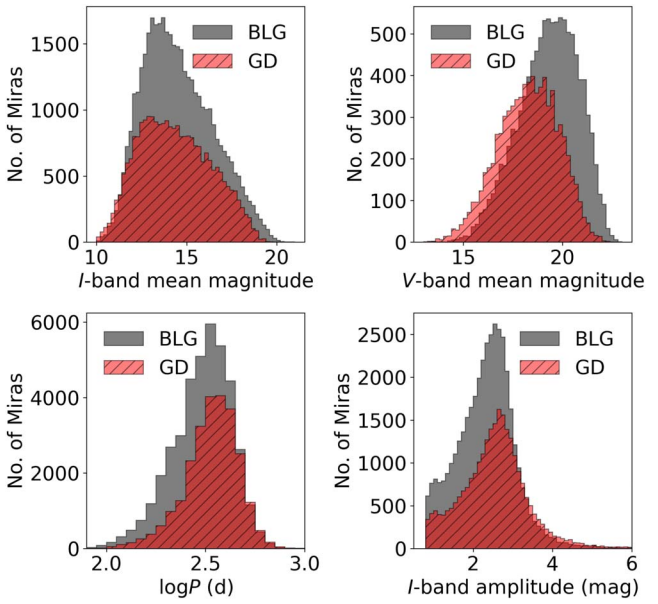

Figure 8. Distributions of the *I*-band mean magnitudes (top left), *V*-band mean magnitudes (top right), pulsation periods (bottom left), and *I*-band amplitudes (bottom right) for the Miras in the BLG (gray histograms) and GD fields (red dashed histograms).

The spectral energy distributions of Miras show maxima around 1–2 μm (see, e.g., Figures 6 and 7 in Iwanek et al. 2021b), therefore the distributions of the *V*-band mean magnitude are shifted toward larger values (top right panel in Figure 8), with maxima at 19.7 mag for Miras in the BLG and 18.5 mag for Miras in the GD. The distribution of the BLG Miras population is shifted toward fainter magnitudes, due to the higher interstellar extinction in this direction and the greater depth of the OGLE photometry in the BLG fields compared to the GD ones.

An interesting feature is presented in the distribution of the pulsation periods (bottom left panel in Figure 8). The GD Mira population has on average longer pulsation periods than the BLG population, which indicates that GD Miras are on average younger than their BLG counterparts (Trabucchi & Mowlavi 2022). The maxima of the pulsation period distributions are at $\log P = 2.52$ ($\sim$331 days) for the BLG population and at $\log P = 2.56$ ($\sim$363 days) for the GD population.

To confirm the statistical significance of the difference between the BLG and GD pulsation period distributions, we compared these distributions using the two-sample, two-sided Kolmogorov–Smirnov (K-S) test, with the null hypothesis that both distributions are similar, against the alternative hypothesis that they are different. As the BLG sample is much larger than the GD one, we randomly chose 25,625 stars from the BLG sample (i.e., the same as the GD sample size) and calculated the K-S test. We repeated the sample drawing and calculation of the K-S test 1000 times, each time obtaining a p-value close to 0. This means that the null hypothesis could be rejected with high probability, leading to the conclusion that the BLG and GD pulsation period distributions are significantly different.

In general, the spiral structure of the Milky Way can be traced by molecular gas (Dame et al. 2001), neutral gas (Burton 1988), star-forming regions (Burns et al. 2014; Reid et al. 2014), or young stars, e.g., classical Cepheids (Skowron et al. 2019a, 2019b; Chen et al. 2019). On the other hand, the second main component of the Milky Way, the bulge, can be traced by red-clump (RC) stars (Weiland et al. 1994; Lopez-Corredoira et al. 1997; Nataf et al. 2010; McWilliam & Zoccali 2010; Wegg & Gerhard 2013; López-Corredoira et al. 2019), RR Lyrae variables (Pietrukowicz et al. 2015; Semczuk et al. 2022), or, finally, Miras (Matsunaga et al. 2009; López-Corredoira 2017; Grady et al. 2020). Recently, Urago et al. (2020) suggested that GD Miras with longer periods probably trace the spiral arms in the Milky Way. It turns out that Mira-type variables, thanks to their wide age range and their being abundant throughout the Milky Way, are extremely valuable tracers of old, intermediate, and young stellar populations.

The distributions of the *I*-band brightness amplitude are cut at 0.8 mag, which is related to the classification method of Miras (see Section 3). Miras in the GD fields have on average larger amplitudes, with the peak of the distribution at 2.7 mag, while the BLG population has a slightly lower amplitude, with the distribution peak at 2.5 mag. It is clearly seen that Miras with *I*-band amplitudes higher than 4 mag are rare. Additionally, it can be noticed that there is a small surplus of GD Miras with *I*-band brightness amplitudes higher than 3 mag.

Miras are usually divided into O-rich and C-rich (Riebel et al. 2010) stars. Soszyński et al. (2005) made such a division for the LMC Miras, based on their position in the optical Wesenheit index versus the NIR Wesenheit index diagram. Unfortunately, the same division could not be used for LPVs in the Milky Way, due to the considerable depth of the BLG and GD along the line of sight (Soszyński et al. 2013). However, our latest research (Iwanek et al. 2021a, P. Iwanek et al. 2022, in preparation) shows that such a division can be made based on pulsation periods and mid-IR color indices.

One of the still unsolved mysteries surrounding the structure of our Galaxy is the existence of the X-shaped bulge. The X-shaped bulge was originally discovered in the RC stars (McWilliam & Zoccali 2010; Nataf et al. 2010). However, there are doubts whether the split in the RC stars along some lines of sight is caused by a geometric effect or whether it depends solely on the different brightness of the two RC star populations (e.g., López-Corredoira et al. 2019). The nearly complete collection of Mira stars, which are also standard candles representing an intermediate-age population, can independently prove or falsify the geometric split of the bulge. López-Corredoira (2017) did not find any evidence for the X-shaped bulge in the Mira variables, but that study was limited to a much smaller sample of Miras than the one presented in this paper. The collection of Miras reported in this paper will be used for a direct examination of the three-dimensional structure of the Galactic bulge.

6. Conclusions

In this paper, we have presented and discussed the largest, purest, and most complete collection of Milky Way Miras published to date. In total, we found 65,981 Mira-type variables in the OGLE databases. The vast majority of this collection (47,532 stars) turned out to be new discoveries, and with this catalog, we have more than tripled the number of known Miras in the Galaxy.

In the catalog, we provide the J2000 equatorial coordinates, pulsation period, *I*-band and *V*-band (if available) mean magnitudes, *I*-band amplitude, cross-identifications with other variable star catalogs, and finding chart for each Mira. We also provide the *I*-band and *V*-band time-series photometry

collected since 1997 during the OGLE-II, OGLE-III, and OGLE-IV sky surveys.

This collection will be the basis for many future studies on the stellar evolution or structure of the Milky Way. We believe that our catalog will contribute to solving the puzzle of the X-shaped bulge. Thanks to the high completeness and purity of the catalog, it can also be used for training machine-learning classification algorithms aimed at the automatic classification of variable stars in large-scale sky surveys.

We would like to thank the anonymous referee for constructive and valuable comments that improved our manuscript. This work has been supported by the National Science Centre, Poland, via grants MAESTRO No. 2016/22/A/ST9/00009 to IS and OPUS 2018/31/B/ST9/00334 to SK. PI is partially supported by Kartezjusz program No. POWR.03.02.00-00-I001/16-00, founded by the National Centre for Research and Development, Poland. This research has made use of the International Variable Star Index (VSX) database, operated at AAVSO, Cambridge, MA, USA.

ORCID iDs

Patryk Iwanek https://orcid.org/0000-0002-6212-7221
Igor Soszyński https://orcid.org/0000-0002-7777-0842
Szymon Kozłowski https://orcid.org/0000-0003-4084-880X
Radosław Poleski https://orcid.org/0000-0002-9245-6368
Paweł Pietrukowicz https://orcid.org/0000-0002-2339-5899
Jan Skowron https://orcid.org/0000-0002-2335-1730
Marcin Wrona https://orcid.org/0000-0002-3051-274X
Przemysław Mróz https://orcid.org/0000-0001-7016-1692
Andrzej Udalski https://orcid.org/0000-0001-5207-5619
Michał K. Szymański https://orcid.org/0000-0002-0548-8995
Dorota M. Skowron https://orcid.org/0000-0001-9439-604X
Krzysztof Ulaczyk https://orcid.org/0000-0001-6364-408X
Mariusz Gromadzki https://orcid.org/0000-0002-1650-1518
Krzysztof Rybicki https://orcid.org/0000-0002-9326-9329
Milena Ratajczak https://orcid.org/0000-0002-3218-2684

References

Alard, C., & Lupton, R. H. 1998, ApJ, 503, 325
Alcock, C., Allsman, R. A., Axelrod, T. S., et al. 1995, AJ, 109, 1653
Arnold, R. A., McSwain, M. V., Pepper, J., et al. 2020, ApJS, 247, 44
Barnes, T. G. I. 1973, ApJS, 25, 369
Battistini, C., & Bensby, T. 2016, A&A, 586, A49
Bellm, E. C., Kulkarni, S. R., Graham, M. J., et al. 2019, PASP, 131, 018002
Berlioz-Arthaud, P. 2003, A&A, 397, 943
Bernhard, A., & Hümmerich, S. 2013, OEJV, 159, 1
Bhardwaj, A., Kanbur, S., He, S., et al. 2019, ApJ, 884, 20
Burns, R. A., Nagayama, T., Handa, T., et al. 2014, ApJ, 797, 39
Burton, W. B. 1988, in Galactic and Extragalactic Radio Astronomy, ed. K. I. Kellermann & G. L. Verschuur (Berlin: Springer-Verlag), 295
Campbell, L. 1955, Studies of Long Period Variables (Cambridge, MA: American Association of Variable Star Observers (AAVSO))
Catchpole, R. M., Robertson, B. S. C., Lloyd Evan, T. H. H., et al. 1979, SAAOC, 1, 61
Catelan, M., & Smith, H. A. 2015, Pulsating Stars (Weinheim: Wiley-VCH)
Chambers, K. C., Magnier, E. A., Metcalfe, N., et al. 2016, arXiv:1612.05560
Chen, X., Wang, S., Deng, L., et al. 2019, NatAs, 3, 320
Chen, X., Wang, S., Deng, L., et al. 2020, ApJS, 249, 18
Dame, T. M., Hartmann, D., & Thaddeus, P. 2001, ApJ, 547, 792
Drake, A. J., Graham, M. J., Djorgovski, S. G., et al. 2014, ApJS, 213, 9
Drake, A. J., Djorgovski, S. G., Catelan, M., et al. 2017, MNRAS, 469, 3688
Flewelling, H. A., Magnier, E. A., Chambers, K. C., et al. 2020, ApJS, 251, 7
Gaia Collaboration, Brown, A. G. A., Vallenari, A., et al. 2018, A&A, 616, A1
Gaia Collaboration, Prusti, T., de Bruijne, J. H. J., et al. 2016, A&A, 595, A1
Glass, I. S., & Feast, M. W. 1982, MNRAS, 199, 245
Glass, I. S., & Lloyd Evans, T. 1981, Natur, 291, 303
Grady, J., Belokurov, V., & Evans, N. W. 2020, MNRAS, 492, 3128
Groenewegen, M. A. T., Nanni, A., Cioni, M. R. L., et al. 2020, A&A, 636, A48
Heinze, A. N., Tonry, J. L., Denneau, L., et al. 2018, AJ, 156, 241
Hertzsprung, E. 1928, BAN, 4, 174
Hinkle, K. H., Hall, D. N. B., & Ridgway, S. T. 1982, ApJ, 252, 697
Hoffleit, D. 1997, JAAVSO, 25, 115
Hogg, E. G. 1933, JRASC, 27, 75
Huang, C. D., Riess, A. G., Hoffmann, S. L., et al. 2018, ApJ, 857, 67
Huang, C. D., Riess, A. G., Yuan, W., et al. 2020, ApJ, 889, 5
Ita, Y., & Matsunaga, N. 2011, MNRAS, 412, 2345
Ita, Y., Menzies, J. W., Whitelock, P. A., et al. 2021, MNRAS, 500, 82
Iwanek, P., Soszyński, I., & Kozłowski, S. 2021a, ApJ, 919, 99
Iwanek, P., Soszyński, I., Skowron, J., et al. 2019, ApJ, 879, 114
Iwanek, P., Kozłowski, S., Gromadzki, M., et al. 2021b, ApJS, 257, 23
Jayasinghe, T., Stanek, K. Z., Kochanek, C. S., et al. 2019, MNRAS, 486, 1907
Keenan, P. C. 1966, ApJS, 13, 333
Keenan, P. C., Garrison, R. F., & Deutsch, A. J. 1974, ApJS, 28, 271
Koval, G. T. 1957, PZ, 12, 108
Kraemer, K. E., Sloan, G. C., Keller, L. D., et al. 2019, ApJ, 887, 82
Kukarkin, B. V. 1957, PZ, 12, 33
Kurtz, D. W. 1985, MNRAS, 213, 773
Lause, F. 1930, JRASC, 24, 271
Lloyd Evans, T. 1976, MNRAS, 174, 169
Lockwood, G. W., & Wing, R. F. 1971, ApJ, 169, 63
Lomb, N. R. 1976, Ap&SS, 39, 447
López-Corredoira, M. 2017, ApJ, 836, 218
Lopez-Corredoira, M., Garzon, F., Hammersley, P., Mahoney, T., & Calbet, X. 1997, MNRAS, 292, L15
López-Corredoira, M., Lee, Y. W., Garzón, F., & Lim, D. 2019, A&A, 627, A3
Maciel, W. J. 1976, A&A, 48, 27
Matsunaga, N., Kawadu, T., Nishiyama, S., et al. 2009, MNRAS, 399, 1709
McWilliam, A., & Zoccali, M. 2010, ApJ, 724, 1491
Menzies, J. W., Whitelock, P. A., & Feast, M. W. 2015, MNRAS, 452, 910
Menzies, J. W., Whitelock, P. A., Feast, M. W., & Matsunaga, N. 2019, MNRAS, 483, 5150
Minniti, D., Lucas, P. W., Emerson, J. P., et al. 2010, NewA, 15, 433
Mowlavi, N., Lecoeur-Taïbi, I., Lebzelter, T., et al. 2018, A&A, 618, A58
Nataf, D. M., Udalski, A., Gould, A., Fouqué, P., & Stanek, K. Z. 2010, ApJL, 721, L28
Nhung, P. T., Hoai, D. T., Tuan-Anh, P., et al. 2022, ApJ, 927, 169
Ou, J.-Y., & Ngeow, C.-C. 2022, AJ, 163, 192
Pepper, J., Pogge, R. W., DePoy, D. L., et al. 2007, PASP, 119, 923
Perrin, G., Ridgway, S. T., Lacour, S., et al. 2020, A&A, 642, A82
Pietrukowicz, P., Dziembowski, W. A., Mróz, P., et al. 2013, AcA, 63, 379
Pietrukowicz, P., Kozłowski, S., Skowron, J., et al. 2015, ApJ, 811, 113
Pojmański, G. 1997, AcA, 47, 467
Reid, M. J., Menten, K. M., Brunthaler, A., et al. 2014, ApJ, 783, 130
Riebel, D., Meixner, M., Fraser, O., et al. 2010, ApJ, 723, 1195
Samus', N. N., Kazarovets, E. V., Durlevich, O. V., Kireeva, N. N., & Pastukhova, E. N. 2017, ARep, 61, 80
Scargle, J. D. 1982, ApJ, 263, 835
Schwarzenberg-Czerny, A. 1996, ApJL, 460, L107
Semczuk, M., Dehnen, W., Schönrich, R., & Athanassoula, E. 2022, MNRAS, 509, 4532
Shappee, B. J., Prieto, J. L., Grupe, D., et al. 2014, ApJ, 788, 48
Skowron, D. M., Skowron, J., Mróz, P., et al. 2019a, Sci, 365, 478
Skowron, D. M., Skowron, J., Mróz, P., et al. 2019b, AcA, 69, 305
Soszyński, I., Udalski, A., Kubiak, M., et al. 2005, AcA, 55, 331
Soszyński, I., Udalski, A., Szymański, M. K., et al. 2009, AcA, 59, 239
Soszyński, I., Udalski, A., Szymański, M. K., et al. 2011, AcA, 61, 217
Soszyński, I., Udalski, A., Szymański, M. K., et al. 2013, AcA, 63, 21
Soszyński, I., Olechowska, A., Ratajczak, M., et al. 2021, ApJL, 911, L22
Trabucchi, M., & Mowlavi, N. 2022, A&A, 658, L1
Udalski, A. 2003, AcA, 53, 291
Udalski, A., Kubiak, M., & Szymanski, M. 1997, AcA, 47, 319
Udalski, A., Szymanski, M., Kaluzny, J., Kubiak, M., & Mateo, M. 1992, AcA, 42, 253
Udalski, A., Szymanski, M. K., Soszynski, I., & Poleski, R. 2008, AcA, 58, 69
Udalski, A., Szymański, M. K., & Szymański, G. 2015, AcA, 65, 1
Urago, R., Omodaka, T., Nagayama, T., et al. 2020, ApJ, 891, 50
Uttenthaler, S., McDonald, I., Bernhard, K., Cristallo, S., & Gobrecht, D. 2019, A&A, 622, A120

VanderPlas, J. T. 2018, ApJS, 236, 16
Watson, C. L., Henden, A. A., & Price, A. 2006, in Society for Astronomical Sciences 25th Annual Symp. (Rancho Cucamonga, CA: Society for Astronomical Sciences), 47
Wegg, C., & Gerhard, O. 2013, MNRAS, 435, 1874
Weiland, J. L., Arendt, R. G., Berriman, G. B., et al. 1994, ApJL, 425, L81
Whitelock, P. A., & Feast, M. W. 2014, in EAS Publications Series 67–68, The Milky Way Unravelled by Gaia: GREAT Science from the Gaia Data Releases, ed. N. A. Walton et al. (Les Ulis: EDP Sciences), 263
Whitelock, P. A., Feast, M. W., Marang, F., & Groenewegen, M. A. T. 2006, MNRAS, 369, 751
Whitelock, P. A., Feast, M. W., Marang, F., & Overbeek, M. D. 1997, MNRAS, 288, 512
Whitelock, P. A., Menzies, J. W., Feast, M. W., & Marigo, P. 2018, MNRAS, 473, 173
Whitelock, P. A., Menzies, J. W., Feast, M. W., Nsengiyumva, F., & Matsunaga, N. 2013, MNRAS, 428, 2216
Whitney, B. S. 1960, AJ, 65, 381
Whitney, C. A. 1975, JAAVSO, 4, 22
Wood, P. R. 1979, ApJ, 227, 220
Wood, P. R., & Cahn, J. H. 1977, ApJ, 211, 499
Woźniak, P. R. 2000, AcA, 50, 421
Yao, Y., Liu, C., Deng, L., de Grijs, R., & Matsunaga, N. 2017, ApJS, 232, 16
Yu, J., Hekker, S., Bedding, T. R., et al. 2021, MNRAS, 501, 5135
Yuan, W., He, S., Macri, L. M., Long, J., & Huang, J. Z. 2017, AJ, 153, 170
Yuan, W., Macri, L. M., Javadi, A., Lin, Z., & Huang, J. Z. 2018, AJ, 156, 112